Evaluation of Waste Office Paper and Waste Newsprint as a Resource for Nanocellulose

Ekrem Durmaz ,* and Saim Ates

Two types of wastepaper and a filter paper as a reference cellulose source were used for nanocellulose production. The production process of cellulose nanofiber (CNF) was conducted *via* mechanical disintegration following TEMPO oxidation, while the sulfuric acid hydrolysis method was applied for cellulose nanocrystal (CNC) production. The equivalent spherical diameters of CNFs were determined as 1520 nm for waste office paper (OP), 4920 nm for waste newsprint (NP), and 2180 nm for filter paper (FP). In contrast, the equivalent spherical diameters of CNCs were found to be 652 nm for OP, 2110 nm for NP, and 1090 nm for FP. The maximum crystallinity index was established to be 96.9% in the FP-CNC sample. Thermal degradation of raw material and deinked fiber samples for three different paper types occurred between 270 and 390 °C. Thermal degradation of CNF and CNC obtained from these paper types measured in the range of 240 to 360 °C and 140 to 600 °C, respectively. The FTIR analysis revealed chemical bond structures, such as O–H, C–H, C–O, C=O, CH_2, C–C, C–O–C, *etc.*, forming in the raw material, deinked fiber, CNF, and CNC of the samples. Especially considering their crystallinity and thermal properties, it can be said that waste office paper is more suitable for nanocellulose production than waste newsprint.

DOI: 10.15376/biores.21.1.2025-2046

Keywords: Cellulose nanofiber (CNF); Cellulose nanocrystal (CNC); Waste paper; Nanocellulose

*Contact information: Kastamonu University, Faculty of Forestry, Department of Forest Industrial Engineering, 37150, Kastamonu, Türkiye; *Corresponding author: edurmaz@kastamonu.edu.tr*

INTRODUCTION

Today's world requires the use of renewable and sustainable technologies in all areas of life due to increasing environmental concerns such as excessive use of fossil resources, climate change, waste management, public health, *etc.* (Thomas *et al.* 2020). Solid waste from mining, industry, homes, and farms has caused significant environmental problems in recent years (Joshi *et al.* 2017). The vast volume of waste paper from offices and newspapers is one of the solid wastes that contribute the most harm to the environment. They are typically neglected and eventually burn or biodegrade slowly (Su *et al.* 2017). According to reports, recycling one ton of waste paper can save about 27 tons of water and 3 tons of wood, thereby significantly and positively affecting the environment and economy (Joshi *et al.* 2015). However, waste paper is challenging to recycle because the paper industry can only reprocess paper so many times until the fiber length shortens and the tensile strength decreases to an excessive degree. In addition, the poor mechanical strength of waste papers creates some disadvantages in their usage in the paper industry. Hence, it has become a worthwhile and difficult task to figure out how to turn these

materials from trash into wealth and use them in novel ways, such as recycling used office paper and newspapers (Joshi *et al.* 2017).

The majority of the cellulosic sources used to isolate nanocellulose come from the agricultural and forest sectors, with a small amount coming from cellulosic waste produced by homes and businesses (Moriana *et al*. 2016; García *et al*. 2017). The forest and agriculture industries have many uses and constraints, leading to increased global interest in waste cellulosic sources. Many types of waste paper play a significant role in the creation of this cellulosic waste. Since there is a significant quantity of cellulosic fraction in this biomass, it is important that the maximum the amount of cellulosic waste that gets recycled. Due to many recycling processes, non-recycled or nonrecyclable cellulosic waste typically deteriorates openly because the paper forms do not produce fibers with the appropriate length and strength (Filson *et al*. 2009; Elliston *et al*. 2015). Open dumping is the root cause of environmental and land use issues. An alternate strategy to steer clear of these issues may be to convert this cellulosic biomass into other value-added products (Mohamed *et al.* 2015; Nishimura *et al.* 2016; Chen and Lee 2018).

Although waste paper can be regarded as a great supply of cellulose for making nanocellulose, there are certain practical obstacles that could prevent this noble alternative method of recycling wastepaper. Since it encompasses a wide range of used paper products, from hard cardboard to extremely delicate tissue paper, the term "wastepaper" is quite complicated in and of itself. The biggest obstacle to using waste paper is obtaining the purest raw materials, which can be accomplished by appropriately separating waste paper at the source. Chemical and mechanical treatment might vary from batch to batch, depending on the type of paper and impurities. The composition and finishing of each variety of paper vary depending on its intended usage. Wastepaper eventually contains pollutants from the ingredients combined during the papermaking process or added for final use. Fillers (kaolin, calcium carbonate, titanium oxide, *etc*.), additives (starch, dyes, sizing agents, dry strength resins, retention aids, drainage aids, *etc*.), plasticizers (benzoates, phthalates, *etc.*), oils (mineral and vegetable), biocides, chelating agents, surfactants, antioxidants, and inks (containing dyes, resins (alkyd, phenolic, polyacrylates, *etc.*) are the most frequent contaminants. Other pollutants that are commonly found in wastepaper include lacquers, food fragments, staples, adhesives, and plastic and aluminum lamination and coverings (Vukoje and Rožić 2018). The aforementioned contaminants must be removed in order to prepare nanocellulose from waste paper efficiently. This is because they cause problems such as the need for additional chemicals for pretreatment and hydrolysis, which slows down the reactions during the preparation process. Mechanical processes (separation and screening for staples, adhesives, plastic lamination, aluminum lamination, and covers) and chemicals (particularly deinking agents like alkaline, sodium silicate, surfactants, *etc*.) are typically used to remove contaminants. Even while wastepaper can be mechanically and chemically treated to remove pollutants, this procedure eventually increases the yield loss, energy consumption, and pollution load on the land and water system. Choosing a single treatment for all waste paper kinds is challenging (Hietala *et al*. 2018).

The decreased viscosity of cellulosic fibers and NFC compared to those achieved with virgin fiber NFC (reference NFC) is another drawback of using wastepaper for nanocellulose. This disadvantage is reflected in strength properties that are 17 to 21% lower than reference NFC (Hietala *et al*. 2018). Wastepaper nanocellulose has certain quality problems even if its morphology—particularly its dimensions—is similar to that of nanocellulose derived from other cellulosic sources. The kind of wastepaper utilized as a

cellulose source and the procedures employed for processing can be expected to have a significant impact on the quality of nanocellulose. The ultimate characteristics and subsequent uses of nanocellulose are adversely affected by the residues of fillers, inks, and lignin that remain in it. Its applicability in fields requiring strong optical qualities, such as papermaking and sophisticated optical materials, is limited by coloring caused by lignin, ink, and other impurities. Its use in creating fire-retardant nanocomposites is limited by its low thermal stability, which in some cases is caused by the presence of sulfate groups (Campano *et al*. 2017b; Adu *et al*. 2018; Chen and Lee 2018).

Cellulose is one of the most renewable natural resources and is comprised of linearly bonded anhydroglucose monomeric units $(C_6H_{10}O_5)_n$. The cellulose polymer naturally includes both crystalline and amorphous regions (Morais *et al.* 2013). Numerous industries, including paper, apparel, adhesives, textiles, food, cosmetics, and medicines, have extensively used cellulose (Kallel *et al.* 2016). The production of nanocellulose types from diverse renewable cellulose-based sources and their usage in technical domains have gained increased attention with the development of nanotechnology. The production of nanocellulose from wastepaper especially has attracted the attention of researchers in the last decade (Campano *et al.* 2017a, 2017b).

The Technical Association of the Pulp and Paper Industry (TAPPI) and multiple concerned bodies have recommended that nanocellulose can be classified into three main groups depending on its morphology (Noremylia *et al.* 2022): 1) more entangled cellulose nanofiber (CNF) (Kępa *et al.* 2019), which are long and flexible existing as interconnected nano-fibrillar structures, 2) short and rigid crystalline rod-like cellulose nanocrystal (CNC) (Ilyas *et al.* 2018), and 3) bacterial nanocellulose (BNC) (Wang *et al.* 2019), which are high in purity and very crystalline. Additionally, some researchers have also introduced another nanocellulose type termed hairy cellulose nanocrystalline (HCNC), featuring protruding cellulose segments from both ends of the crystalline body (Van De Ven and Sheikhi 2016). The CNF is typically several micrometers long, containing a combination of amorphous and crystalline zones. It is composed of fibrils having a diameter of 5 to 100 nm. By contrast, CNC is 100 to 500 nm long and 2 to 20 nm wide, with crystalline needle-like structures (Picot-Allain and Emmambux 2023; Sarangi *et al.* 2024). Mechanical disintegration methods, such as high-pressure homogenization, micro-fluidization, micro-grinding, high-intensity ultrasonication, ball-milling, high-speed shearing, high-speed stirring, cryocrushing, and steam explosion, have been applied in the production of CNF (Randhawa *et al.* 2022; Xu *et al.* 2024). In contrast, different acid hydrolysis processes, such as formic acid, hydrochloric acid, phosphoric acid, sulfuric acid, sulfuric acid/acetic acid, and sulfuric/oxalic acid extraction have been commonly used to prepare CNC (Hossen *et al.* 2024).

Nanocellulose, which can have outstanding features, such as non-toxic nature, superior biocompatibility, high aspect ratio, advanced biodegradability, high crystallinity, good optical properties, transparency, excellent mechanical strength, low density, low thermal expansion, tailorable surface chemistry, *etc.*, can be acquired from various cellulose-based biomaterials such as wood pulp, non-woody plant and fruit or agricultural waste, marine animals, bacteria, and algae (Hossen *et al.* 2024; Norizan *et al.* 2022; Poulose *et al.* 2022). Because of its superior properties mentioned above, nanocellulose has been utilized in many different industries, including biomedical, packaging, paper and board, automotive, electronic, cosmetic, food, sensors, water filtration, fuel cell, construction, tissue engineering, 3D printing, healthcare, polymer composites, oilfield servicing fluids, drug delivery systems, aerogels, and hydrogels (Norizan *et al.* 2022; Kassie *et al.* 2024;

Sarangi *et al.* 2024). Some surface modification methods, such as esterification, silylation, TEMPO-mediated oxidation, sulfonation, etherification, phosphorylation, urethanization, amidation, click chemistry, polymer grafting, and non-covalent surface modification, have been applied to nanocellulose to provide potential application in different industries and to eliminate drawbacks like hydrophilicity, poor interfacial adhesion, agglomeration, *etc.* (Habibi 2014; Ghasemlou *et al.* 2021).

This study aimed to produce cellulose nanofiber (CNF) and cellulose nanocrystal (CNC) from waste office paper (OP), waste newsprint (NP), and filter paper (FP) as a reference source. The morphological, thermal, crystalline properties, zeta potentials, and chemical bond structures of the obtained nanocellulose types were investigated and compared with studies in the literature. Thus, the usage potential and possibilities of these kinds of waste papers in nanocellulose production were introduced.

EXPERIMENTAL

Materials

In this study, waste OP, waste NP, and Whatman Grade 4 FP were used as raw materials in the production of CNF and CNC. Both WP and FP were provided by the Department of Forest Industrial Engineering Laboratories, Kastamonu University. Waste NP was supplied from Kastamonu province. NaOH and NaClO were used in the deinking of waste papers. TEMPO (2,2,6,6-tetramethylpiperidin-1-yl)oxyl, NaBr, ethanol, HCl, chloroform, and distilled water were used in CNF production; the H_2SO_4, distilled water, centrifuge tubes and dialysis tubes with Dalton molecular weight of 12000 to 14000 used in CNC production as well as all laboratory glassware and consumables were supplied by the several distributors of Sigma-Aldrich® and Thermo Fisher Scientific Inc. in Türkiye. Whatman FP used in CNF and CNC production were supplied by Kimeks Chemicals and Health Products Trade Inc., the distributor of Whatman™, in Türkiye. In addition, the production of CNF and CNC suspensions was performed in this laboratory. The analyses for characterizations of CNF and CNC were conducted in Kastamonu University Central Research Laboratory, Erciyes University Nanotechnology Research Center, and Eskisehir Osmangazi University the Center Research Laboratory Application and Research Center.

Methods

Deinking of waste papers

For deinking of waste papers, the method involving alkali and bleaching processes applied by Hasan *et al.* (2023) and Guan *et al.* (2021) for removing ink from WP and NP was used with some modifications. First, approximately 20 g of OP and NP were cut to 5 × 5 mm^2. Samples were then immersed in distilled water and left overnight. The suspension consisting of waste paper particles was mixed with a high-speed mixer for 2 to 3 min to be fiberized and turned into paper pulp. The resulting pulp was filtered using a 100-mesh screen. This process was repeated several times to thoroughly separate the fibers in the waste paper pulp. Then, the pulp samples were first treated in a 5% NaOH suspension, purified, washed with pure water, and then soaked in a 5% NaOH/10% H_2O_2/10% Na_2SiO_3 suspension at 60 °C for 90 min. The pulp/chemical suspension ratio was set at 1:15 (g/mL). The pulps, after the deinking process, were filtered and washed with distilled water until their pH values became neutral. Finally, the pulps were dried at 80 °C for 8 h.

The production of CNF

For CNF production, the method applied by Boufi and Chaker (2016) was conducted. TEMPO oxidation was carried out at pH 10; NaClO was used as the oxidation agent, and TEMPO was used as the catalyst. A total of 2 g of cellulosic pulp was immersed in 200 mL of distilled water. Next, 30 mg TEMPO and 250 mg NaBr were added to it. The oxidation process started after adding 50 mL of NaClO (12% available chlorine) solution. A total of 0.1 M NaOH was added to the suspension to keep the pH at 10 during oxidation. After 1 h, the oxidation process was stopped by adding 20 mL of ethanol, and 0.1 M HCl was added to adjust the pH to 7. After the oxidation process, centrifugation was applied to purify the suspension. This process was carried out at 5000 rpm for 10 min and 4 repetitions. In the last stage of this method, TEMPO-oxidized cellulosic pulp was made at 1% concentration. The suspension was converted into CNF with the help of a high-speed blender with a 1.8 L container capacity (Karaca Inox Powermix Smoothie Blender 1801, 1800 W) at 20000 rpm for 30 min. A few drops of chloroform were added to the CNF suspension to prevent any bacterial or fungal growth. In Fig. 1, the steps conducted in CNF production is demonstrated.

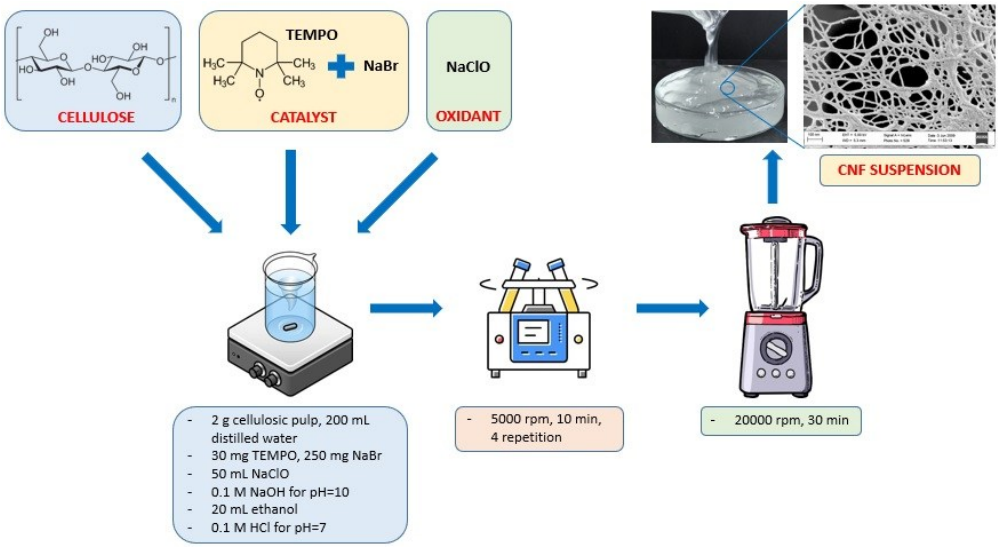

Fig. 1. The steps conducted in CNF production

The production of CNC

The acid hydrolysis process as specified by Lamaming *et al.* (2015) was conducted, such that sulfuric acid was used in the CNC production. Cellulosic pulps were treated in a 64% sulfuric acid solution. The pulp/acid ratio was set at 1:10 (g/mL) and hydrolysis process was carried out in a fume hood at 50 °C for 1 h. The reaction was stopped by adding distilled water to the system at 5 times the pulp/acid volume. Then, the suspension was placed in a centrifuge and processed at 5000 rpm for 10 min. The centrifugation process was repeated 5 times. After each repetition, the supernatant in the tubes was replaced with distilled water. After centrifugation, the supernatant and precipitate in the tubes were mixed for 15 min using a mechanical mixer to obtain a homogeneous suspension. The homogenized CNC suspension was transferred to dialysis tubes with a molecular weight cutoff of 12000 to 14000 Daltons for dialysis, and these tubes were immersed in distilled water as well as kept in the distilled water until their pH reached 7 (approximately 7 to 10 days). The distilled water used was renewed every day. After dialysis, a second

centrifugation process was performed with the same parameters as the first, in 2 repetitions, to remove acid residues in the CNC suspension. Finally, the suspension was ultrasonicated in an ultrasonic bath at a frequency of 53 kHz for 15 min to separate the aggregated CNC particles. The processes applied in the obtaining of CNC is presented in Fig. 2.

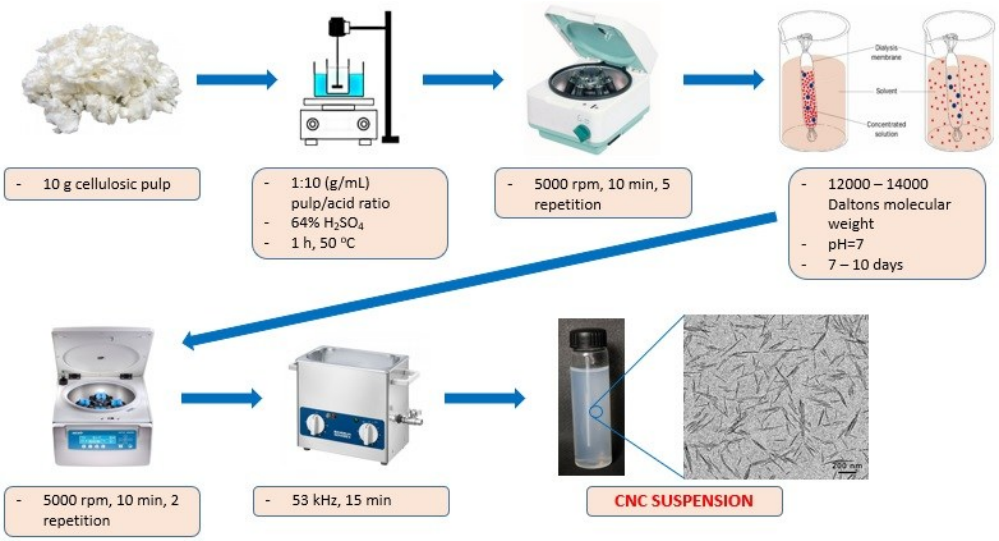

Fig. 2. The processes applied in the obtaining of CNC

Characterization of CNF and CNC

Dynamic light scattering analysis

Dynamic light scattering (DLS) analysis was performed for the morphological evaluation of CNF and CNC samples. Although this analysis is generally applied to nanoparticles with spherical morphology, it also provides information on the particle size distributions of CNF and CNC. Suspensions with a concentration of 0.1% were used for DLS analysis with a DLS measurement device (Nano ZS90; Malvern, UK). The measurements were carried out at the Erciyes University Nanotechnology Application and Research Center.

Zeta potential analysis

Zeta potential values of CNF and CNC were determined with a zeta potential measurement device (Nano ZS90; Malvern, UK) at 0.1% concentration. The measurements were carried out at the Erciyes University Nanotechnology Application and Research Center.

Scanning electron microscopy (SEM) analysis

For morphological examination of the raw material, deinked fiber, and CNF samples, a scanning electron microscope (SEM, Quanta FEG 250, USA) located in Kastamonu University Central Research Laboratory was used. Before imaging, CNF suspensions were diluted to a concentration of 0.01% and dried with a vacuum dryer. The samples were coated with gold for 2 min using a sputter coater (Sputter Coater 108 Auto; Cressington, Watford, UK) before imaging.

Transmission electron microscopy (TEM) analysis

A JEOL 1220 JEM (JEOL Ltd., Tokyo, Japan) transmission electron microscope (TEM) located in the Application and Research Center of Eskişehir Osmangazi University Central Research Laboratory was used for imaging CNF and CNC samples. Because TEM analysis provides information about the delicate structures of tiny samples, raw material and deinked fiber samples were not included in this analysis. Before analysis, the concentrations of CNF suspensions were diluted to 0.05%, while those of CNC were 0.005%, and these suspensions were placed on formvar films supported by copper TEM grids, using a micropipette. The prepared grids were used for imaging.

X-ray diffraction analysis

The crystallinity index (CI) determines the orientation of cellulose crystals in a fiber concerning the fiber axis. The CI is detected by the values given by the 2θ angle near 22º and 18º in X-ray diffraction (XRD) analysis. The crystalline portions of the cellulosic material are represented by 22º, while the amorphous portions are represented by 18º. Consequently, the following formula is used to determine the samples' crystallinity index (Reddy and Yang 2005):

$$\text{CI (\%)} = \frac{I_{22} - I_{18}}{I_{22}} \text{ x } 100 \quad (1)$$

In Eq. 1, I_{22} and I_{18} symbolize the intensity values at the 2θ angles obtained near 22° and 18°, respectively. The crystallinity properties of the samples were determined with a Bruker D8 Advance (Billerica, MA, USA) brand X-ray diffraction device at the Kastamonu University Central Research Laboratory. This analysis was carried out using CuKα radiation at a wavelength of λ = 0.15418 nm, with a 2θ value in the range of 5 to 80°. Additionally, diffraction data were obtained at 2θ = 0.05° step spacing and 3 s/step time.

Fourier transform infrared spectroscopy (FTIR) analysis

The chemical bond structures of the samples were determined using the Bruker Alpha FTIR device (Billerica, MA, USA) at the Kastamonu University Central Research Laboratory. Each sample was analyzed at a scanning resolution of 4 cm^{-1} and a band range of 4000 to 650 cm^{-1}.

Thermogravimetric analysis (TGA)

The samples' thermal characteristics were ascertained using the TGA apparatus (TGA-DTA Hitachi STA7300; Tokyo, Japan), located in the Kastamonu University Central Research Laboratory. Tests were carried out between 25 and 800 °C in an air and nitrogen gas atmosphere, with a temperature increase of 10 °C each minute.

Differential scanning calorimetry (DSC) analysis

In addition to TGA analysis, DSC analysis was also used to determine the thermal properties of the samples. These tests were done using a Hitachi DSC7020 (Tokyo, Japan) DSC apparatus, located at the Kastamonu University Central Research Laboratory. Nitrogen gas was used with a temperature increase of 10 °C per minute between 25 and 400 °C.

RESULTS AND DISCUSSION

Zeta Potentials and Size Distributions of CNF and CNC

The zeta potentials and conductivities of the CNF samples were found to be -37.5 mV and 0.365 mS/cm for OP, -7.17 mV and 0.144 mS/cm for NP, and -33.2 mV and 0.792 mS/cm for FP, respectively, while the zeta potentials and conductivities of the CNC samples were found to be -55.5 mV and 0.0597 mS/cm for OP, -23.6 mV and 2.01 mS/cm for NP, and -65.2 mV and 0.0620 mS/cm for FP, respectively. According to these results, the zeta potential values of CNC samples generally were more negative than those of CNFs.

In addition, the equivalent spherical diameters of the CNF samples were determined as 1520 nm, 4920 nm, and 2180 nm for OP, NP, and FP, respectively, whereas the equivalent spherical diameters of the CNC samples were determined as 652 nm, 2110 nm, and 1090 nm for OP, NP, and FP, respectively.

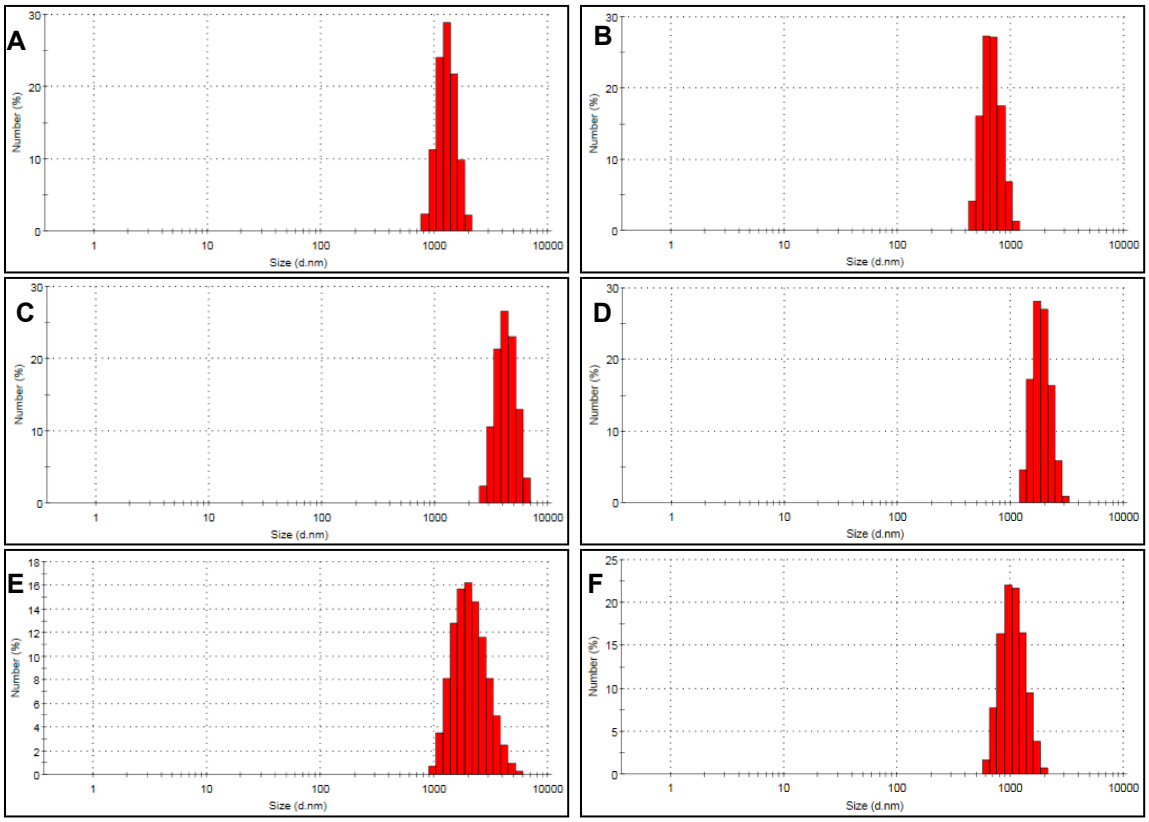

Fig. 3. Dimensional distributions of CNF and CNC samples A) OP-CNF, B) OP-CNC, C) NP-CNF, D) NP-CNC, E) FP-CNF, and F) FP-CNC

DLS analysis is a practical tool for estimating how the particle dimensions of nanomaterials are distributed. In this approach, the nanomaterials are modelled as spheres in Brownian motion, measuring the particles' hydrodynamic radius (RH) 21, which is equivalent to the translational diffusion coefficient of the particles. Although the aforementioned particles are not spherical, this analysis is very useful in showing the dimensional distributions of nanoparticles (Hasan *et al*. 2023). The dimensional distributions of CNF and CNC samples produced from various paper types are indicated in Fig. 3. Huang *et al.* (2021) produced CNF with different chemical pre-treatment from office waste paper and bleached pulp board as well as examined their average dimensions

and zeta potentials. For different CNF samples, it was found that the average dimensions ranged between 17.1 and 31.9 nm, and zeta potentials ranged between -19.0 and -41.9 mV. In another study, Hasan *et al.* (2023) obtained CNC with sulfuric acid hydrolysis for 4 and 6 h of waste newspapers. The zeta potential of CNC, obtained as a result of 4 h of acid hydrolysis, was found to be -3.9 mV, while the zeta potential of CNC, which was obtained as a result of 6 h of acid hydrolysis, was determined to be -8.2 mV.

Morphological Properties

The SEM images of CNF and CNC obtained from different paper types and raw materials and deinked samples of these papers are given in Fig. 4. There is no SEM image of the FP specimen because it was not deinked. Moreover, the TEM images of these nanocellulose types are presented in the same figure. It can be seen from SEM images of waste papers and deinked pulp that the fibrillation process worked well with the bleaching process of deinked pulps, especially for OP. The deinking process not only removed ink from raw materials, but it also separated the cellulosic pulp fibers. When the CNF and CNC samples of the papers were examined, it was determined that the CNFs exhibited a spiderweb-like structure, while the CNCs had a needle- or rice grain-shaped structure. This is because mechanical fibrillation applied to deinked pulps after TEMPO oxidation transformed the fibrous structure of the pulp samples into a network form. The reason why CNCs have a needle-shaped structure is that as a result of acid hydrolysis, the amorphous regions of OP, NP, and FP cellulose are removed, leaving behind the crystalline regions of the cellulose. These structures of CNFs and CNCs are also clearly visible in the TEM pictures of the samples. In addition, the equivalent spherical diameters of the CNF samples were found to be 1520 nm, 4920 nm, and 2180 nm for OP, NP, and FP, respectively, whereas the equivalent spherical diameters of the CNC samples were found to be 652 nm, 2110 nm, and 1090 nm for OP, NP, and FP, respectively. Lei *et al.* (2024) produced rod-shaped and spherical-shaped nanocellulose from office waste paper under different enzymatic hydrolysis conditions. They confirmed that the diameter of rod-shaped nanocellulose was in the range of 40 to 200 nm, and the diameter of spherical-shaped nanocellulose was between 20 and 50 nm after morphological analysis. Jiang *et al.* (2020) acquired CNC from waste office paper by sulfuric acid hydrolysis and ammonium persulfate oxidation methods. As a result of morphological analysis, the researchers revealed that the length of sulfuric acid-CNC was 200 ± 25 nm, and its diameter was 8 ± 2.5 nm, whereas the length of ammonium persulfate-CNC was 130 ± 15 nm, and its diameter was 4 ± 2.5 nm.

Crystallinity

The crystallinity results of OP, NP, and FP samples are given in Fig. 5. The peak at 22° on the 2θ-scale axis of the graphs demonstrates the crystalline regions of the samples, whereas the peak at 18° reflects the amorphous regions of the samples. Furthermore, the crystallinity indexes of the samples as raw material, deinked fiber, CNF, and CNC are presented in Table 1. It is apparent that the deinking process increased the crystallinity index of OP and NP. At the same time, it was determined that the crystallinity indexes of CNF and CNC obtained from different types of paper were higher than the raw material and deinked samples of these papers.

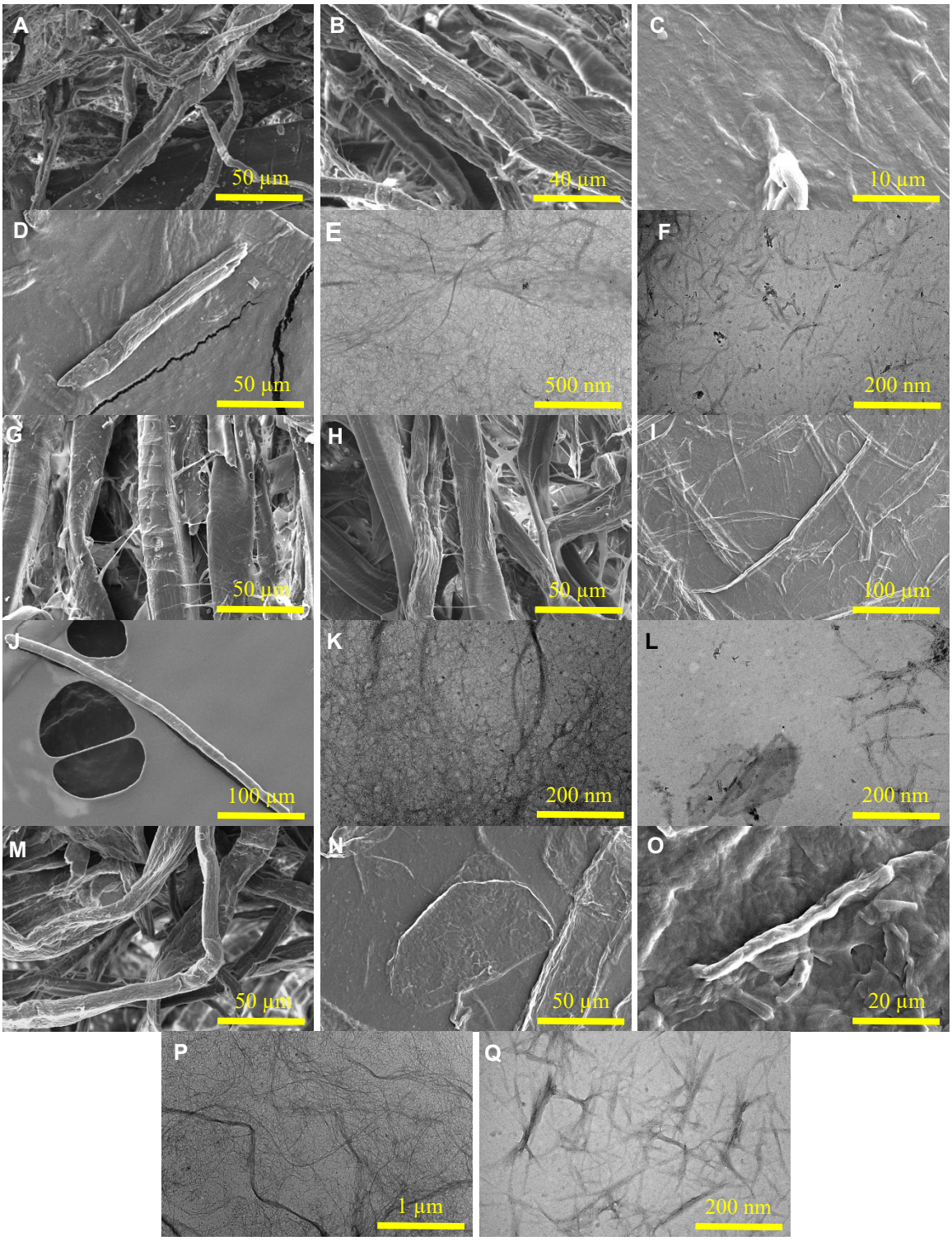

Fig. 4. Morphology of A) OP-Raw material (SEM), B) OP-Deinked fiber (SEM), C) OP-CNF (SEM), D) OP-CNC (SEM), E) OP-CNF (TEM), F) OP-CNC (TEM), G) NP-Raw material (SEM), H) NP-Deinked fiber (SEM), I) NP-CNF (SEM), J) NP-CNC (SEM), K) NP-CNF (TEM), L) NP-CNC (TEM), M) FP-Raw material (SEM), N) FP-CNF (SEM), O) FP-CNC (SEM), P) FP-CNF (TEM), and Q) FP-CNC (TEM)

Among the different types of paper, the highest crystallinity indexes were found in CNC samples of the papers. This was due to the sulfuric acid hydrolysis applied in CNC production, which removes the amorphous regions of cellulose, leaving only the crystalline regions. Additionally, the maximum crystallinity index was determined as 96.9% in CNC produced from FP.

The reason for this is thought to be that the FP is already produced from pure cellulose and is not subjected to any deinking process. Jiang *et al.* (2020) found the crystallinity index of the waste office paper, used in CNC production to be 68.8% in terms of raw material.

On the one hand, the crystallinity index of the sulfuric acid-CNC and ammonium persulfate-CNC were confirmed as 77.6% and 72.4%, respectively. In another study, Danial *et al.* (2015) revealed the crystallinity properties of CNC produced from old newspaper. They found the crystallinity index as 65.8% for waste paper, 91% for pure cellulose, and 75.9% for CNC.

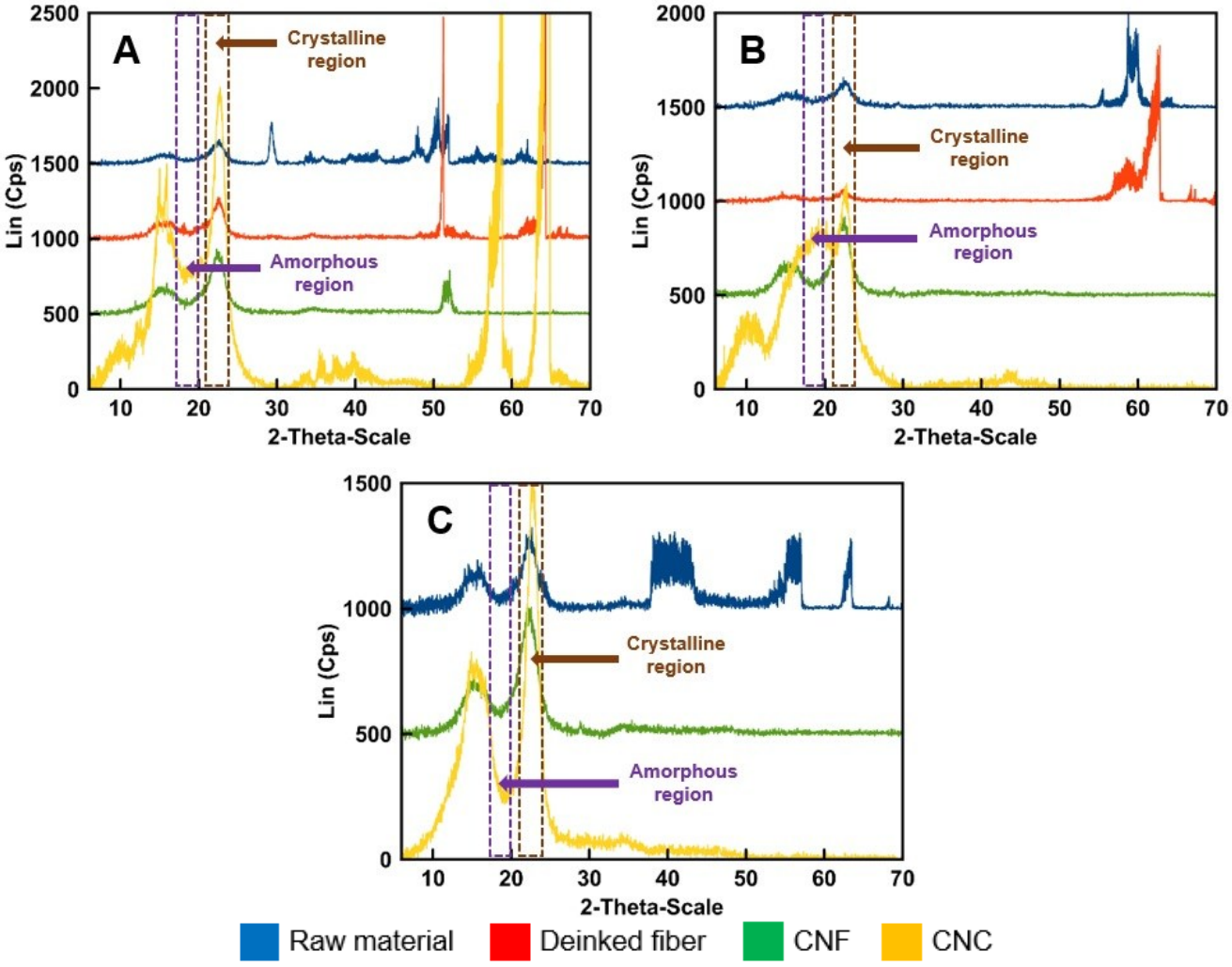

Fig. 5. XRD results of A) OP B) NP, and C) FP

Table 1. Crystallinity Indexes of the Samples as Raw Material, Deinked Fiber, CNF, and CNC

Samples	Crystallinity Index (%)
OP – raw material	65.30
OP – deinked fiber	92.57
OP – CNF	93.84
OP – CNC	95.00
NP – raw material	64.51
NP – deinked fiber	85.75
NP – CNF	91.42
NP – CNC	92.68
FP – raw material	85.65
FP – CNF	87.32
FP – CNC	96.90

Thermal Properties

The thermal properties of OP, NP, and FP samples as raw material, deinked fiber, CNF and CNC are shown in TGA graphs. The mass loss up to 100 °C in the TGA graphs of all paper types is due to the removal of moisture in the samples. According to Fig. 6A, it was determined that thermal decompositions for OP occurred between approximately 300 and 380 °C in raw material; between 300 and 380 °C in deinked fiber; between 250 and 360 °C in CNF; and between 170 and 600 °C in CNC. After thermal degradation, approximately 40% of the residual material was released from OP raw material, 20% from deinked fiber, 30% from CNF, and 35% from CNC. When the TGA analysis results of OP were examined, it was observed that the raw material and deinked samples exhibited better thermal properties than the CNF and CNC samples. It was also observed that the weight loss was greater in the deinked sample. The CNC sample began to decompose at lower temperatures compared to the other samples. The reason for this is thought to be that the CNC sample does not contain amorphous regions of cellulose but consists only of crystalline regions, and that the sulfate groups on the CNC surface also cause this situation. The CNF sample exhibited better thermal resistance than CNC, but its thermal degradation occurred at lower temperatures compared to the raw material and deinked fiber samples. It was determined that the raw material and deinked fiber samples had better thermal properties compared to nanocellulose types because they were not subjected to any mechanical or chemical treatment and contained both crystalline and amorphous regions of cellulose. While the thermal degradation of raw material, deinked fiber, and CNF samples occurred in a narrow temperature range, the thermal degradation of CNC occurred in a wide temperature range and took a long time.

Zhang *et al.* (2019) investigated the thermal properties of spherical nanocellulose produced from waste kraft paper and printed paper. They stated that the onset decomposition temperature and the temperature at the maximum weight loss of the bleached pulp were 238 and 338 °C, respectively, whereas those of nanocellulose were 262 and 353 °C. Orue *et al.* (2017) examined the thermal features of CNCs obtained from office waste paper *via* different methods. They stated that all samples exhibited a weight loss below 130 °C, corresponding to the evaporation of water. In addition, the onset degradation temperature of nonprinted paper, totally printed paper, CNC-1, and CNC-2 samples were found as 301, 259, 277, and 200 °C, respectively.

Figure 6B shows the TGA results explaining the thermal degradation of NP samples. It was determined that the degradation of the samples occurred between approximately 270 and 390 °C for the raw material; between 270 and 380 °C for the deinked fiber; between 250 and 360 °C for CNF; and between 160 and 600 °C for CNC. As a result of thermal degradation, approximately 20%, 30%, 35%, and 40% of residue material was released from the raw material, deinked fiber, CNF, and CNC samples, respectively. The thermal properties of the raw material, deinked fiber, and CNF samples of NP were close to each other and exhibited a different thermal property than CNC. Although more residual material was released in the CNC sample after thermal decomposition, this sample type started to decompose at much lower temperatures compared to the others, and the decomposition process took longer. As in the OP-CNC sample, thermal degradation in the NP-CNC sample occurred over a wider temperature range compared to the others. The crystalline and amorphous regions contained in the raw material, deinked fiber, and CNF samples ensured that these samples exhibited better thermal properties than the CNC sample consisting of only crystalline regions. In their study examining the thermal properties of nanocellulose obtained under different enzymatic hydrolysis conditions, Lei *et al.* (2024) declared that the weight of samples decreased slightly due to the loss of water at temperatures below 100 °C and for recycled waste paper fiber and types of nanocellulose, most TGA curves showed a dramatic weight loss at 270 to 360 °C, which was caused by the important decomposition of cellulose. Huang *et al.* (2021) prepared CNF with various chemical pre-treatment from office waste paper and bleached pulp board. They indicated that the decomposition peaks in the temperature range of 246 to 290 °C were mainly caused by the breakage of cellulose glycosidic bonds and the thermal depolymerization of the residual hemicellulose, whereas the decomposition peaks located in the temperature region of 290 to 313 °C were mainly due to the depolymerization of the cellulose structure. Moreover, residual rates of CNFs were found between 28.3% and 31.0%.

The TGA analysis results of the FP samples are presented in Fig. 6C. Because no deinking process was applied to the FP, there is no example of the FP as deinked fiber in this graph. It was determined that the degradation of the FP samples occurred between approximately 300 and 380 °C for raw material, between 240 and 350 °C for CNF, and between 140 and 600 °C for CNC. The residue material amounts were determined as approximately 20% for raw material, 30% for CNF, and 35% for CNC. When the TGA graph of the FP samples was examined, it was seen that the FP-raw material sample, as in the other two paper types, exhibited better thermal properties than the CNF and CNC samples. The fact that the FP-raw material sample showed better thermal resistance than the nanocellulose samples is because the raw material had not been subjected to any mechanical or chemical treatment, and the fact that CNF showed better thermal resistance than CNC is because, unlike CNC, CNF has both amorphous and crystalline regions of cellulose. Similar to OP and NP, the thermal degradation of the FP-CNC sample also occurred over a wide temperature range. However, as a result of this thermal decomposition, the amount of residue in the CNC sample was found to be higher than the amount of residue in both the raw material and CNF samples. In their study investigating the thermal properties of CNF obtained from waste paper, Joshi and Chauhan (2024) determined the onset of degradation of untreated paper, bleached paper, and CNF as 273.3, 283.5, and 206.4 °C, respectively. Furthermore, it was stated that weight loss at 550 °C was 79.3% for untreated paper, 86.4% for bleached paper, and 48.9% for CNF. Jiang *et al.* (2020) confirmed the maximum temperature of thermal degradation of raw waste office

paper, sulfuric acid-CNC, and ammonium persulfate-CNC as 334, 207, and 324 °C, respectively. Moreover, the carbon residues at 700 °C were found to be 16.1% for raw waste office paper, 26.7% for sulfuric acid-CNC, and 14.2% for ammonium persulfate-CNC.

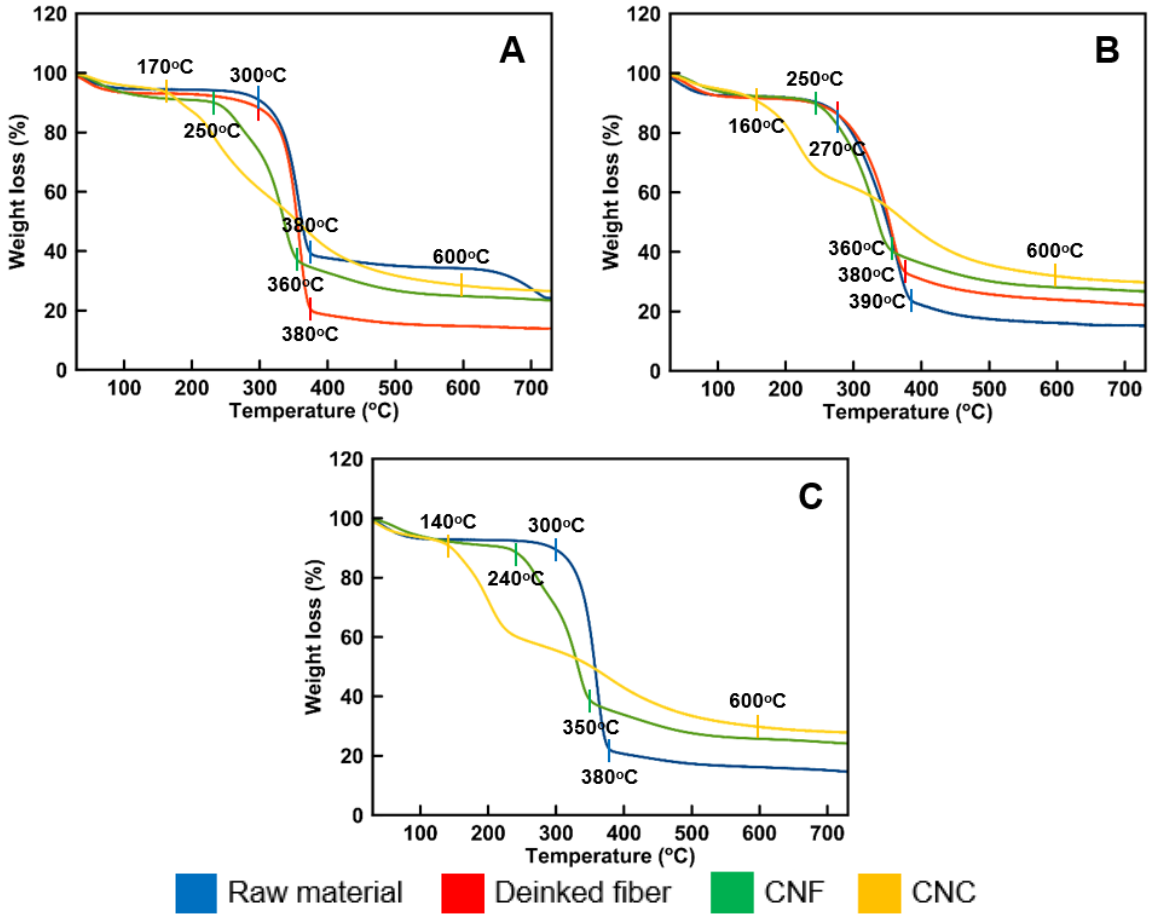

Fig. 6. TGA results of A) OP, B) NP, and C) FP

In Fig. 7, the DSC results of OP, NP, and FP as raw material, deinked fiber, CNF, and CNC are presented. These DSC graphs provide information about the glass transition temperatures of the samples. The endothermic curves detected between 50 and 150 °C in the DSC graphs of the samples were formed due to the evaporation of moisture in the samples. The main thermal decomposition of all samples occurred above 200 °C. According to the DSC graph of OP samples, all samples exhibited a distinct endothermic curve within the examined temperature range, and this endothermic peak indicates the melting of the sample. The peaks that clearly appear around 100 °C in the raw material and deinked fiber samples are due to the removal of moisture absorbed in these samples. As observed in the OP samples, endothermic curves were also apparent in the DSC graph of the NP samples. The endothermic curves detected between 100 and 150 °C were formed due to the evaporation of moisture in the samples. The main decomposition of the NP samples occurred between 200 and 250 °C. The removal of moisture from the raw material, CNF, and CNC samples is the cause of the first endothermic curves in the FP's DSC graph, which appeared between 100 and 150 °C. Lei *et al.* (2024) reported that a small endothermic peak was seen around 100 °C, which was caused by the evaporation of water

according to the DSC graph. In addition, it was remarked that most nanocellulose samples and recycled waste paper fiber showed relatively obvious endothermic peaks near 356 and 349.4 °C, respectively. In another study, Lei *et al.* (2018) investigated the thermal properties of CNCs produced at different sulfuric acid concentrations. The researchers revealed that the onset degradation temperatures of CNCs ranged from 125 to 231 °C, which were lower than the onset degradation temperatures of deinked office waste pulp.

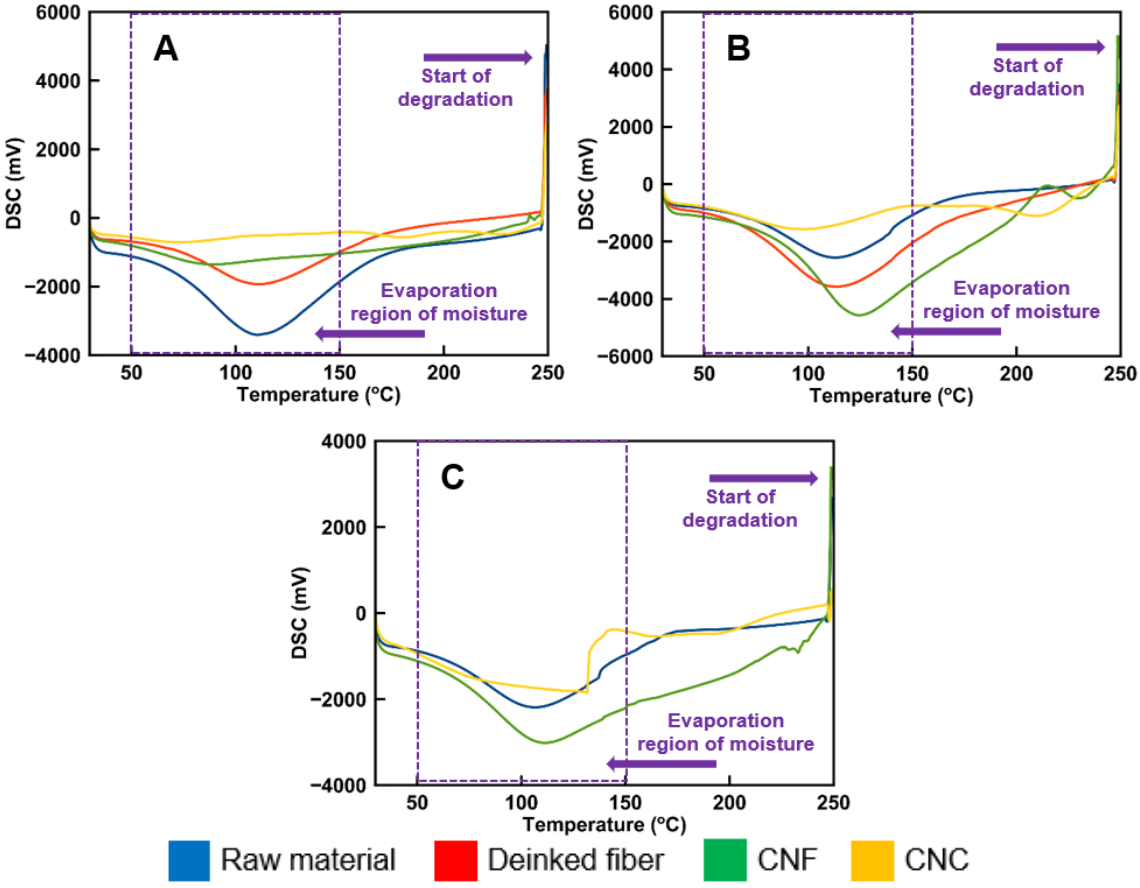

Fig. 7. DSC results of A) OP, B) NP, and C) FP

Chemical Bond Structures

The FTIR results explaining the bond structures of OP, NP, and FP as raw material, deinked fiber, CNF, and CNC are presented in Fig. 8. According to the results of OP FTIR analysis, the peaks appearing at frequencies of 3282, 3387, 3335, and 3329 cm^{-1} in raw material, deinked fiber, CNF, and CNC samples, respectively, represent the free O–H stretching vibrations of OH groups in cellulose molecules (Huang *et al.* 2021). Detected peaks between 2870 and 2900 cm^{-1} in the same samples correspond to the C–H stretching vibrations of the alkyl groups in aliphatic bonds (Joshi and Chauhan 2024). The vibrations determined around 1640 cm^{-1} in the raw material, deinked, and CNC samples are attributed to the O–H bond of the absorbed water (Hasan *et al.* 2023). The peaks appearing at 1315 cm^{-1} and 1027 cm^{-1} in the raw material sample and at 1314 cm^{-1} and 1029 cm^{-1} in the deinked fiber sample belong to the stretching of C–O (acyl) and C–O (alkoxy) bonds in the cellulose structure, respectively (Yu *et al.* 2022). The peaks at 1052 cm^{-1} in the raw material and 1051 cm^{-1} in CNF reflect the stretching vibrations of the C–O–C pyranose ring. The

vibrations seen at 895 and 896 cm^{-1} in the same samples represent the glycosidic C_1–O–C_4 structure of the β-glycosidic bond in cellulose (De Souza *et al.* 2017). The vibration encountered at a frequency of approximately 1000 cm^{-1} in CNC is attributed to the C–O bond (Herrera *et al.* 2017). In the same sample, the peak at 1334 cm^{-1} indicates the CH_2 bond in the crystal regions, while the peak at 1314 cm^{-1} indicates the CH_2 vibration in cellulose (Vaez and Asadpour 2022). The peaks seen at 1160 and 1104 cm^{-1} in the CNC sample reveal C–C ring bond and C–O–C glycosidic ether bond seen in polysaccharides, respectively (Lei *et al.* 2018). In the CNF sample, the vibration detected at a frequency of 1425 cm^{-1} reflects the asymmetric CH_2 bond in the crystal region of cellulose, and the vibration detected at a frequency of 1159 cm^{-1} reflects the C–C ring bond that occurs due to the polysaccharide components (Van-Pham *et al.* 2020). The peak at 1660 cm^{-1} in the deinked fiber indicates C=O strain in cellulose, whereas the peak at 1605 cm^{-1} in CNF indicates C=O strain in the carboxyl group (Yu *et al.* 2022).

According to the results of NP FTIR analysis, the peaks detected at 3334 cm^{-1} in the raw material, 3330 cm^{-1} in the deinked fibers, 3325 cm^{-1} in CNF, and 3332 cm^{-1} and 3283 cm^{-1} in CNC reflect the O–H bonds of the hydroxyl groups in the structure of cellulose (Joshi and Chauhan 2024). The vibrations determined at frequencies of 1631 cm^{-1} and 1639 cm^{-1} in the raw material and CNC samples, respectively, are attributed to the absorption of water molecules (Guan *et al.* 2021). The peaks appearing at frequencies of 2914, 2914, 2889, and 2898 cm^{-1} in the raw material, deinked fiber, CNF, and CNC samples, respectively, correspond to the C–H stretching vibrations of alkyl groups in aliphatic bonds (Orue *et al.* 2017). The peaks seen at 1314 cm^{-1} in the deinked fiber, CNF, and CNC samples indicate the C–O (acyl) bonds of cellulose, while the peaks seen at 1027 cm^{-1} and 1028 cm^{-1} indicate the C–O (alkoxy) bonds of cellulose, respectively (Yu *et al.* 2022). The vibration occurring at a frequency of 2358 cm^{-1} in the raw material sample indicates the presence of the C=O bond formed by cellulose due to CO_2 adsorption from the standard atmosphere. This is explained by the Lewis acid-base interaction (Van-Pham *et al.* 2020). The CH_2 peaks detected at 1422 and 1425 cm^{-1} in the raw material and CNC samples, respectively, correspond to the bending vibrations in the crystal regions of cellulose (Vaez and Asadpour 2022). The peaks detected at 1156, 1158, and 1159 cm^{-1} in the raw material, deinked fiber, CNF, and CNC samples are attributed to the C–C ring bond seen in polysaccharides (Huang *et al.* 2021). The vibrations that were determined at frequencies of 1054 cm^{-1} in raw material, 1053 cm^{-1} in deinked fibers, 1051 cm^{-1} in CNF, and 1053 cm^{-1} in CNC represent the C–O–C pyranose ring stretching (Kano *et al.* 2019). Similarly, it is stated that the vibrations at frequencies of 1104, 1105, 1102, and 1103 cm^{-1} in raw material, deinked fiber, CNF, and CNC samples, respectively, belong to the C–O–C glycosidic ether bonds in the polysaccharide components (Lei *et al.* 2018).

According to the results of FTIR analysis of FP samples, all vibrations detected between the frequencies of 3200 and 3600 cm^{-1} reflect the O–H bonds found in cellulose (Egamberdiev and Norboyev 2022). The vibrations occurring at frequencies of 2889, 2898, and 2893 cm^{-1} in the raw material, CNF, and CNC samples, respectively, are associated with the C–H stretching of the alkyl groups in the aliphatic bonds (Peretz *et al.* 2019). The peaks observed at 1029 cm^{-1} in raw material and CNC as well as at 1021 cm^{-1} in CNF correspond to the C–O/C–C stretching of cellulosic structures (Putro *et al.* 2019). Whereas the peaks detected at frequencies of 1313 and 1314 cm^{-1} of the samples indicate the CH_2 bonds in cellulose (Vaez and Asadpour 2022), the peaks detected at frequencies of 1423, 1425, and 1427 cm^{-1} demonstrate the bending vibrations of the CH_2 bonds in the crystal regions of cellulose (Van-Pham *et al.* 2020). The peaks at 1159 and 1160 cm^{-1} in CNF and

CNC samples, respectively, represent the C–C ring bonds in the polysaccharide components, while the peaks at 895 and 896 cm^{-1} reflect the characteristic β-(1–4) glycosidic bonds of cellulose (Guan *et al.* 2021).

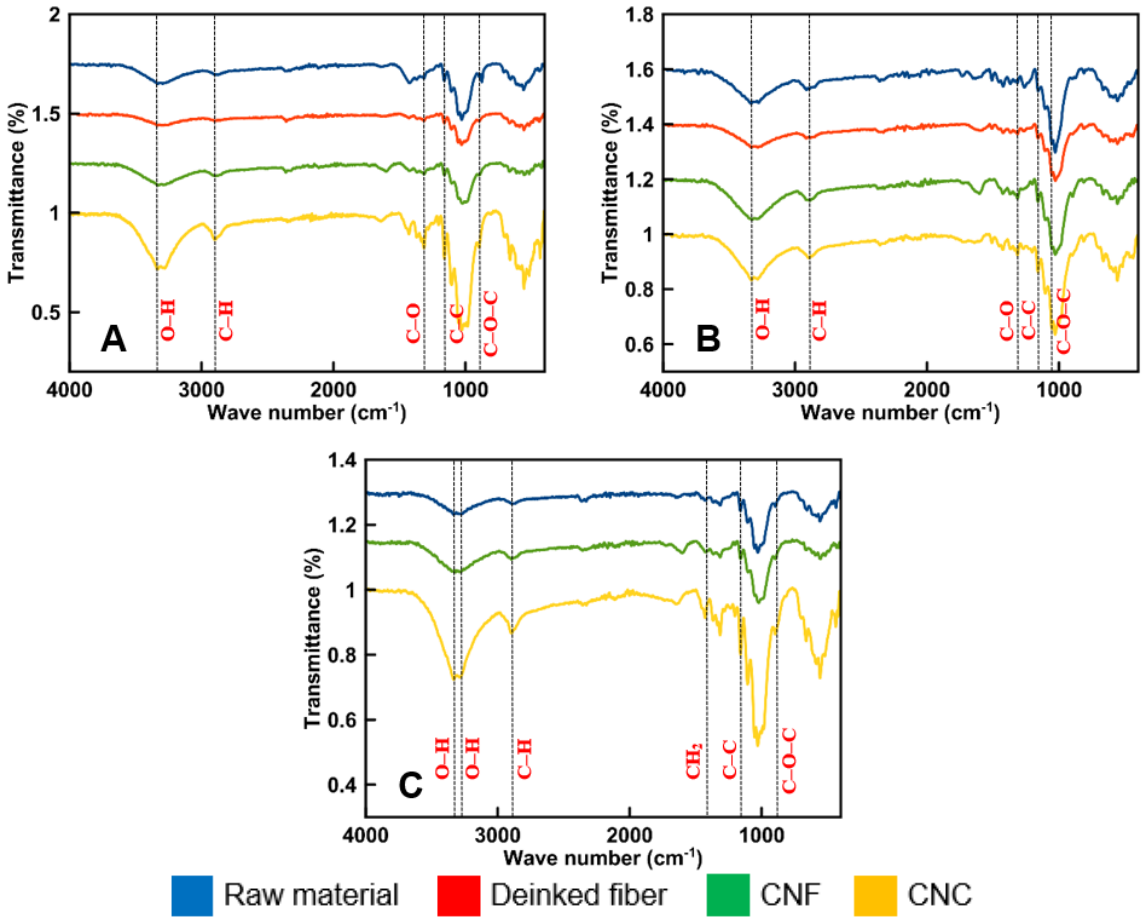

Fig. 8. FTIR results of A) OP, B) NP, and C) FP

CONCLUSIONS

1. As a result of the study, it was revealed that the nanocellulose types produced from waste office paper and waste newsprint had similar properties when compared to those produced from filter paper and different cellulosic raw materials in the literature.
2. The most negative zeta potential was found to be -65.2 mV in the cellulose nanocrystal specimens prepared from filter paper (FP-CNC). Meanwhile, the maximum equivalent spherical diameter was determined as 4920 nm in the NP-CNF sample, and the minimum equivalent spherical diameter was confirmed as 652 nm in the CNC specimen made from waste office paper (OP-CNC).
3. The scanning electron microscope (SEM) and transmission electron microscope (TEM) analyses showed that CNC samples had a rice-like structure and CNF samples had a web-like structure.

4. The crystallinity index of CNC was observed to be higher than that of CNF, and the highest crystallinity index was determined to be 96.9% in the FP-CNC sample.
5. Thermal degradation of raw material and deinked fiber samples happened between 270 and 390 °C, whereas thermal degradation of CNFs and CNCs occurred in the range of 240 °C to 360 °C and 140 °C to 600 °C, respectively.
6. Chemical bond structures, including O–H, C–H, C–O, C=O, CH_2, C–C, C–O–C, *etc.*, that compose the raw material, deinked fiber, CNF, and CNC of the samples were identified using Fourier transform infrared (FTIR) analysis.

ACKNOWLEDGMENTS

The authors would like to acknowledge The Scientific and Technological Research Council of Türkiye (Türkiye Bilimsel ve Teknolojik Araştırma Kurumu, Project Number: 223O405) for financial support. Additionally, appreciation is extended to Kastamonu Aycan Packaging & Industrial Cleaning Products Inc., Kastamonu, Türkiye; OYKA Paper Packaging Industry and Trade Inc., Zonguldak, Türkiye; Gözüm Trading Inc., Zonguldak, Türkiye; the scholars and technicians from Kastamonu University Central Research Laboratory, Kastamonu, Türkiye; Erciyes University Nanotechnology Research Center, Kayseri, Türkiye; Eskisehir Osmangazi University Center Research Laboratory Application and Research Center, Eskişehir, Türkiye and Kahramanmaraş Sütçü İmam University Faculty of Forestry Forest Industry Engineering, Kahramanmaraş, Türkiye for their valuable supports.

REFERENCES CITED

Adu, C., Jolly, M., and Thakur, V. K. (2018). "Exploring new horizons for paper recycling: a review of biomaterials and biorefinery feedstocks derived from wastepaper," *Curr. Opin. Green Sustain. Chem*. 13, 21-26. https://doi.org/10.1016/j.cogsc.2018.03.003

Boufi, S., and Chaker, A. (2016). "Easy production of cellulose nanofibrils from corn stalk by a conventional high speed blender," *Ind. Crop. Prod.* 93, 39-47. https://doi.org/10.1016/j.indcrop.2016.05.030

Campano, C., Merayo, N., Balea, A., Tarrès, Q., Delgado-Aguilar, M., Mutjé, P., Negro, C., and Blanco, Á. (2017a). "Mechanical and chemical dispersion of nanocelluloses to improve their reinforcing effect on recycled paper," *Cellulose* 25(1), 269-280. https://doi.org/10.1007/s10570-017-1552-y

Campano, C., Miranda, R., Merayo, N., Negro, C., and Blanco, Á. (2017b). "Direct production of cellulose nanocrystals from old newspapers and recycled newsprint," *Carbohydr. Polym.* 173, 489-496. https://doi.org/10.1016/j.carbpol.2017.05.073

Chen, Y. W., and Lee, H. V. (2018). "Revalorization of selected municipal solid wastes as new precursors of ''green" nanocellulose via a novel one-pot isolation system: a source perspective," *Int. J. Biol. Macromol*. 107, 78-92. https://doi.org/10.1016/j.ijbiomac.2017.08.143

Danial, W. H., Majid, Z. A., Muhid, M. N. M., Triwahyono, S., Bakar, M. B., and Ramli, Z. (2015). "The reuse of wastepaper for the extraction of cellulose nanocrystals," *Carbohydr. Polym.* 118, 165-169. https://doi.org/10.1016/j.carbpol.2014.10.072

De Souza, A. G., Kano, F. S., Bonvent, J. J., and dos Santos Rosa, D. (2017). "Cellulose nanostructures obtained from waste paper industry: A comparison of acid and mechanical isolation methods," *Mater. Res.* 20(2), 209-214. https://doi.org/10.1590/1980-5373-MR-2016-0863

Egamberdiev, E. A., and Norboyev, S. K. (2022). "Extraction of cellulose nanocrystals from secondary paper waste and their use in paper production," *Tech. Sci. Innov.* 3, 215-222. https://doi.org/10.51346/tstu-01.22.3-77-0195

Elliston, A., Wilson, D.R., Wellner, N., Collins, S.R., Roberts, I.N., and Waldron, K.W. (2015). "Effect of steam explosion on waste copier paper alone and in a mixed lignocellulosic substrate on saccharification and fermentation," *Bioresour. Technol.* 187, 136-143. https://doi.org/10.1016/j.biortech.2015.03.089

Filson, P. B., Dawson-Andoh, B. E., and Schwegler-Berry, D. (2009). "Enzymatic-mediated production of cellulose nanocrystals from recycled pulp," *Green Chem*. 11(11), 1808-1814. https://doi.org/10.1039/b915746h

García, A., Labidi, J., Belgacem, M. N., and Bras, J. (2017). "The nanocellulose biorefinery: woody versus herbaceous agricultural wastes for NCC production," *Cellulose* 24(2), 693-704. https://doi.org/10.1007/s10570-016-1144-2

Ghasemlou, M., Daver, F., Ivanova, E. P., Habibi, Y., and Adhikari, B. (2021). "Surface modifications of nanocellulose: From synthesis to high-performance nanocomposites," *Prog. Polym. Sci.* 119, article 101418. https://doi.org/10.1016/j.progpolymsci.2021.101418

Guan, Y., Li, W., Gao, H., Zhang, L., Zhou, L., and Peng, F. (2021). "Preparation of cellulose nanocrystals from deinked waste newspaper and their usage for papermaking," *Carbohydr. Polym. Technol. Appl.* 2, article 100107. https://doi.org/10.1016/j.carpta.2021.100107

Habibi, Y. (2014). "Key advances in the chemical modification of nanocelluloses," *Chem. Soc. Rev.* 43, 1519-1542. https://doi.org/10.1039/c3cs60204d

Hasan, Z., Zubair, M. O., and Hassan, T. (2023). "Synthesis and characterization of cellulose nanomaterials from waste newspapers," *Mater. Proc.* 14(74), 1-8. https://doi.org/10.3390/IOCN2023-14731

Herrera, M. A., Mathew, A. P., and Oksman, K. (2017). "Barrier and mechanical properties of plasticized and cross-linked nanocellulose coatings for paper packaging applications," *Cellulose* 24(9), 3969-3980. https://doi.org/10.1007/s10570-017-1405-8

Hietala, M., Varrio, K., Berglund, L., Soini, J., and Oksman, K. (2018). "Potential of municipal solid waste paper as raw material for production of cellulose nanofibers," *Waste Manage*. 80, 319-326. https://doi.org/10.1016/j.wasman.2018.09.033

Hossen, M. T., Kundu, C. K., Pranto, B. M. R. R., Rahi, M. S., Chanda, R., Mollick, S., Siddique, A. B., and Begum, H. A. (2024). "Synthesis, characterization, and cytotoxicity studies of nanocellulose extracted from okra (*Abelmoschus esculentus*) fiber," *Heliyon* 10, article e25270. https://doi.org/10.1016/j.heliyon.2024.e25270

Huang, D., Hong, H., Huang, W., Zhang, H., and Hong, X. (2021). "Scalable preparation of cellulose nanofibers from office waste paper by an environment-friendly method," *Polymers* 13(18), article 3119. https://doi.org/10.3390/polym13183119

Ilyas, R. A., Sapuan, S. M., and Ishak, M. R. (2018). "Isolation and characterization of nanocrystalline cellulose from sugar palm fibres (*Arenga pinnata*)," *Carbohydr. Polym.* 181, 1038-1051. https://doi.org/10.1016/j.carbpol.2017.11.045

Jiang, Q., Xing, X., Jing, Y., and Han, Y. (2020). "Preparation of cellulose nanocrystals based on waste paper via different systems," *Int. J. Biol. Macromol.* 149, 1318-1322. https://doi.org/10.1016/j.ijbiomac.2020.02.110

Joshi, G., Naithani, S., Varshney, V. K., Bisht, S. S., Rana, V., and Gupta, P. K. (2015). "Synthesis and characterization of carboxymethyl cellulose from office waste paper: A greener approach towards waste management," *Waste Manag.* 38, 33-40. https://doi.org/10.1016/j.wasman.2014.11.015

Joshi, G., Naithani, S., Varshney, V. K., Bisht, S. S., and Rana, V. (2017). "Potential use of waste paper for the synthesis of cyanoethyl cellulose: A cleaner production approach towards sustainable environment management," *J. Clean. Prod.* 142, 3759-3768. https://doi.org/10.1016/j.jclepro.2016.10.089

Joshi, G., and Chauhan, S. S. (2024). "Synthesis and characterization of cellulose nanofibers from waste paper and their utilization in wood adhesion," *Polym. Compos.* 45, 9103-9118. https://doi.org/10.1002/pc.28397

Kallel, F., Bettaieb, F., Khiari, R., García, A., Bras, J., and Chaabouni, S. E. (2016). "Isolation and structural characterization of cellulose nanocrystals extracted from garlic straw residues," *Ind. Crop. Prod.* 87, 287-296. https://doi.org/10.1016/j.indcrop.2016.04.060

Kano, F. S., De Souza, A. G., and dos Santos Rosa, D. (2019). "Variation of the milling conditions in the obtaining of nanocellulose from the paper sludge," *Rev. Mater.* 24(3), article e20190071. https://doi.org/10.1590/S1517-707620190003.0719

Kassie, B. B., Daget, T. M., and Tassew, D. F. (2024). "Synthesis, functionalization, and commercial application of cellulose-based nanomaterials," *Int. J. Biol. Macromol.* 278, article 134990. https://doi.org/10.1016/j.ijbiomac.2024.134990

Kępa, K., Chaléat, C. M., Amiralian, N., Batchelor, W., Grøndahl, L., and Martin, D. J. (2019). "Evaluation of properties and specific energy consumption of spinifex-derived lignocellulose fibers produced using different mechanical processes," *Cellulose* 26, 6555-6569. https://doi.org/10.1007/s10570-019-02567-x

Lamaming, J., Hashim, R., Sulaiman, O., Leh, C. P., Sugimoto, T., and Nordin, N. A. (2015). "Cellulose nanocrystals isolated from oil palm trunk," *Carbohydr. Polym.* 127, 202-208. https://doi.org/10.1016/j.carbpol.2015.03.043

Lei, W., Fang, C., Zhou, X., Yin, Q., Pan, S., Yang, R., Liu, D., and Ouyang, Y. (2018). "Cellulose nanocrystals obtained from office waste paper and their potential application in PET packing materials," *Carbohydr. Polym.* 181, 376-385. https://doi.org/10.1016/j.carbpol.2017.10.059

Lei, W., Gao, Y., Fang, C., Li, Z., Zhou, X., Li, L., and Pu, M. (2024). "Controllable preparation and morphology regulation of nanocelluloses from waste paper by a green hydrolysis method," *Int. J. Biol. Macromol.* 280, article 135658. https://doi.org/10.1016/j.ijbiomac.2024.135658

Mohamed, M. A., Salleh, W. N. W., Jaafar, J., Asri, S. E. A. M., and Ismail, A. F. (2015). "Physicochemical properties of 'green' nanocrystalline cellulose isolated from recycled newspaper," *RSC Adv.* 5(38), 29842-29849. https://doi.org/10.1039/c4ra17020b

Morais, J. P., Rosa, M. F., de Souza Filho, M. S., Nascimento, L. D., do Nascimento, D. M., and Cassales, A. R. (2013). "Extraction and characterization of nanocellulose

structures from raw cotton linter," *Carbohydr. Polym.* 91(1), 229-235. https://doi.org/10.1016/j.carbpol.2012.08.010

Moriana, R., Vilaplana, F., and Ek, M. (2016). "Cellulose nanocrystals from forest residues as reinforcing agents for composites: a study from macro-to nano-dimensions," *Carbohydr. Polym*. 139, 139-149. https://doi.org/10.1016/j.carbpol.2015.12.020

Nishimura, H., Tan, L., Sun, Z. Y., Tang, Y. Q., Kida, K., and Morimura, S. (2016). "Efficient production of ethanol from waste paper and the biochemical methane potential of stillage eluted from ethanol fermentation," *Waste Manage*. 48, 644-651. https://doi.org/10.1016/j.wasman.2015.11.051

Noremylia, M. B., Hassan, M. Z., and Ismail, Z. (2022). "Recent advancement in isolation, processing, characterization and applications of emerging nanocellulose: A review," *Int. J. Biol. Macromol.* 206, 954-976. https://doi.org/10.1016/j.ijbiomac.2022.03.064

Norizan, M. N., Shazleen, S. S., Alias, A. H., Sabaruddin, F. A., Asyraf, M. R. M., Zainudin, E. S., Abdullah, N., Samsudin, M. S., Kamarudin, S. H., and Norrahim, M. N. F. (2022). "Nanocellulose-based nanocomposites for sustainable applications: A review," *Nanomater.* 12(19), article 3483. https://doi.org/10.3390/nano12193483

Orue, A., Santamaria-Echart, A., Eceiza, A., Peña-Rodriguez, C., and Arbelaiz, A. (2017). "Office waste paper as cellulose nanocrystal source," *J. Appl. Polym. Sci.* 134, article 45257. https://doi.org/10.1002/app.45257

Peretz, R., Sterenzon, E., Gerchman, Y., Vadivel, V. K., Luxbacher, T., and Mamane, H. (2019). "Nanocellulose production from recycled paper mill sludge using ozonation pretreatment followed by recyclable maleic acid hydrolysis," *Carbohydr. Polym.* 216, 343-351. https://doi.org/10.1016/j.carbpol.2019.04.003

Picot-Allain, M. C. N., and Emmambux, M. N. (2023). "Isolation, characterization, and application of nanocellulose from agro-industrial by-products: A review," *Food Rev. Int.* 39(2), 941-969. https://doi.org/10.1080/87559129.2021.1928689

Poulose, A., Parameswaranpillai, J., George, J. J., Gopi, J. A., Krishnasamy, S., Dominic, C. D. M., Hameed, N., Salim, N. V., Radoor, S., and Sienkiewicz, N. (2022). "Nanocellulose: A fundamental material for science and technology applications," *Molecules* 27(22), Article ID 8032. https://doi.org/10.3390/molecules27228032

Putro, J. N., Santoso, S. P., Soetaredjo, F. E., Ismadji, S., and Ju, Y. H. (2019). "Nanocrystalline cellulose from waste paper: Adsorbent for azo dyes removal," *Environ. Nanotechnol. Monit. Manag.* 12, Article ID 100260. https://doi.org/10.1016/j.enmm.2019.100260

Randhawa, A., Dutta, S. D., Ganguly, K., Patil, T. V., Patel, D. K., and Lim, K. T. (2022). "A review of properties of nanocellulose, its synthesis, and potential in biomedical applications," *Appl. Sci.* 12(14), Article ID 7090. https://doi.org/10.3390/app12147090

Reddy, N., and Yang, Y. (2005). "Structure and properties of high quality natural cellulose fibers from cornstalks," *Polymer* 46, 5494-5500. https://doi.org/10.1016/j.polymer.2005.04.073

Sarangi, P. K., Srivastava, R. K., Sahoo, U. K., Singh, A. K., Parikh, J., Bansod, S., Parsai, G., Luqman, M., Shadangi, K. P., Diwan, D., Lanterbecq, D., and Sharma, M. (2024). "Biotechnological innovations in nanocellulose production from waste biomass with a focus on pineapple waste," *Chemosphere* 349, article 140833. https://doi.org/10.1016/j.chemosphere.2023.140833

Su, H., Zhu, P., Zhang, L., Zhou, F., Li, G., Li, T., Wang, Q., Sun, R., and Wong, C. (2017). "Waste to wealth: A sustainable and flexible supercapacitor based on office waste paper electrodes," *J. Electroanal. Chem.* 786, 28-34. https://doi.org/10.1016/j.jelechem.2017.01.002

Thomas, P., Duolikun, T., Rumjit, N. P., Moosavi, S., Lai, C. W., Bin Johan, M. R., and Fen, L. B. (2020). "Comprehensive review on nanocellulose: Recent developments, challenges and future prospects," *J. Mech. Behav. Biomed. Mater.* 110, article 103884. https://doi.org/10.1016/j.jmbbm.2020.103884

Vaez, K., and Asadpour, G. (2022). "Effects of HCl hydrolyzed cellulose nanocrystals from waste papers on the hydroxypropyl methylcellulose/cationic starch biofilms," *Waste Biomass Valor.* 13, 2035-2051. https://doi.org/10.1007/s12649-021-01651-3

Van de Ven, T. G. M., and Sheikhi, A. (2016). "Hairy cellulose nanocrystalloids: A novel class of nanocellulose," *Nanoscale* 8, 15101-15114. https://doi.org/10.1039/c6nr01570k

Van-Pham, D. T., Pham, T. Y. N., Tran, M. C., Nguyen, C. N., and Tran-Cong-Miyata, Q. (2020). "Extraction of thermally stable cellulose nanocrystals in short processing time from waste newspaper by conventional acid hydrolysis," *Mater. Res. Express* 7, article 065004. https://doi.org/10.1088/2053-1591/ab9668

Vukoje, M., and Rožić, M. (2018). "Various valorisation routes of paper intended for recycling–A review," *Cellul. Chem. Technol*. 52(7–8), 515-541.

Wang, J., Tavakoli, J., and Tang, Y. (2019). "Bacterial cellulose production, properties and applications with different culture methods – A review," *Carbohydr. Polym.* 219, 63-76. https://doi.org/10.1016/j.carbpol.2019.05.008

Xu, Y., Wu, Z., Li, A., Chen, N., Rao, J., and Zeng, Q. (2024). "Nanocellulose composite films in food packaging materials: A review," *Polymers* 16(03), article 423. https://doi.org/10.3390/polym16030423

Yu, R., Prabhakar, M. N., Lee, D. W., and Song, J. (2022). "Extraction and characterization of nanocellulose from local waste paper egg trays," *J. Nat. Fibers* 19(14), 8582-8592. https://doi.org/10.1080/15440478.2021.1964143

Zhang, S., Zhang, F., Jin, L., Liu, B., Mao, Y., Liu, Y., and Huang, J. (2019). "Preparation of spherical nanocellulose from waste paper by aqueous NaOH/thiourea," *Cellulose* 26, 5177-5185. https://doi.org/10.1007/s10570-019-02434-9

Article submitted: August 19, 2025; Peer review completed: October 11, 2025; Revised version received: October 27, 2025; Further revised version received: October 28, 2025; Accepted: December 4, 2025; Published: January 16, 2026.
DOI: 10.15376/biores.21.1.2025-2046